S0013-4651(99)09-090-4 CCC: $7.00 © The Electrochemical Society, Inc.

Postexposure Delay Effect on Linewidth Variation in Base Added Chemically Amplified Resist

Chin-Yu Ku,[a] Jia-Min Shieh,[b] Tsann-Bim Chiou,[b] Hwang-Kuen Lin,[c] and Tan Fu Lei[a,z]

[a]*Department of Electronics Engineering and Institute of Electronics, National Chiao Tung University, Hsinchu 300, Taiwan*
[b]*National Nano Device Laboratories, Hsinchu 300, Taiwan*
[c]*Vanguard International Semiconductor Corporation, Hsinchu 300, Taiwan*

To elucidate the linewidth variation caused by postexposure delay (PED) in resist films, the distribution of photogenerated acid, the role of additional base component, and the effect of exposure energy were investigated in *tert*-butoxycarbonyl protected-type chemically amplified positive deep ultraviolet resist. The resist system included an *N*-methyl pyrrolidone organic base which was evaluated via KrF excimer laser lithography. Using various line-and-space patterns formed with a KrF scanner, this work also investigated the change of linewidth caused by the delay time between exposure and postexposure bake. Experimental results indicate that the linewidth broadened immediately following exposure and became a constant value rather than continuously expanding for various pattern sizes. Based on the mechanism of neutralizing organic base and photogenerated acid, a model was established to describe the linewidth according to PED time. Moreover, the effect of exposure energy on linewidth variation was investigated to not only assess the influence of exposure energy but also clarify the relationship between linewidth broadening and delay time. Experimental analysis demonstrates that the exposure latitude and depth of focus can be improved by employing PED.
© 2000 The Electrochemical Society. S0013-4651(99)09-090-4. All rights reserved.

Manuscript submitted September 23, 1999; revised manuscript recieved March 8, 2000.

Chemically amplified resist based on acid catalysis for deep UV lithography is a promising technology for patterns of 0.18 μm or less. To improve the process stability and resist performance, extensive efforts have been made to understand how each component in resist formation influences lithographic performance.[1-13] Previously, the main problems for deep ultraviolet (DUV) resists were airborne contamination and linewidth change with different delay times. For the positive DUV resist, the generation of "T-top" at the resist-air interface is attributed to neutralization of the photogenerated acid by airborne organic bases, such as ammonia, during postexposure delay (PED). Employing a carbon filtration system, overcoat films and pretreating the substrate, can minimize the effects of contamination.[1-5] Linewidth variation is mainly induced by the effect of acid diffusion during exposure and baking. Therefore, the diffusion behavior of photogenerated acid has been widely investigated for both high and low activation energy (*Ea*) resist systems.[7-20] Adding base additives has been reported to reduce linewidth slimming of low *Ea* system such as acetal-based resists owing to reducing acid diffusion.[7,21] To stabilize the latent acid image of high *Ea* resist systems such as *tert*-butoxycarbonyl (t-BOC) containing resins, an additional base component was added not only to quench photogenerated acid, but also to suppress the acid diffusion reaction within the resist film.[8] Theoretical studies have also indicated that limited diffusion is essential for achieving high resolution chemically amplified DUV resists.[26,27]

While inherent resist characteristics such as acid diffusion behavior, the effect of base components, and phenomenon of linewidth variation have been widely studied, presently no relationship has been established for these three components. This work evaluated the influence of organic base additive on acid concentration and lithographic performance in t-BOC-protected type chemically amplified positive DUV resist. A resist system comprising of a chemically amplified positive resist and an organic base, such as *N*-methyl pyrrolidone (NMP), not only prevents a T-top formation, but also suppresses acid diffusion reaction within resist film.[1] Based on the mechanism of neutralization of organic base and photogenerated acid, a model is established herein to describe the behavior of linewidth variation. Furthermore, a very useful equation has also been derived based on the diminution of photogenerated acid in resist film. This equation can accurately predict linewidth variation based on the delay time for various pattern sizes.

The concentration of photogenerated acid is defined by the aerial image of the resist by a power equal to the reaction order of the acid. Therefore, the effect of exposure energy was investigated to clarify the behavior of linewidth variation during postexposure delay. The simulation result, calculated from the lithographic modeling tool PROLITH/2, has been used to evaluate exposure energy dependence on linewidth variation. The clear relationship between linewidth broadening and additional organic base was obtained based on theoretical derivation and experimental analysis.

This investigation assessed how postexposure delay (PED) affects exposure latitude (EL) and depth of focus (DOF). Utilizing the characteristic of postexposure delay can extend the EL and DOF for both 0.18 and 0.22 μm line-and-space patterns.

Experimental

Materials and processing.—The influence of an additional base component, *N*-methyl pyrrolidone (NMP), was investigated in t-BOC-protected type chemically amplified positive DUV resist. The

[z] E-mail: tflei@cc.nctu.edu.tw

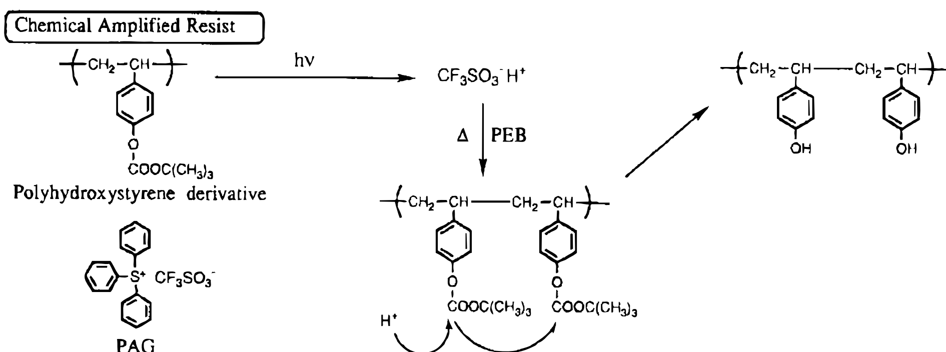

Figure 1. Schematic view of the photolysis of onium salt.

Downloaded on 2014-04-28 to IP 140.113.38.11 address. Redistribution subject to ECS terms of use (see ecsdl.org/site/terms_use) unless CC License in place (see abstract).

S0013-4651(99)09-090-4 CCC: $7.00 © The Electrochemical Society, Inc.

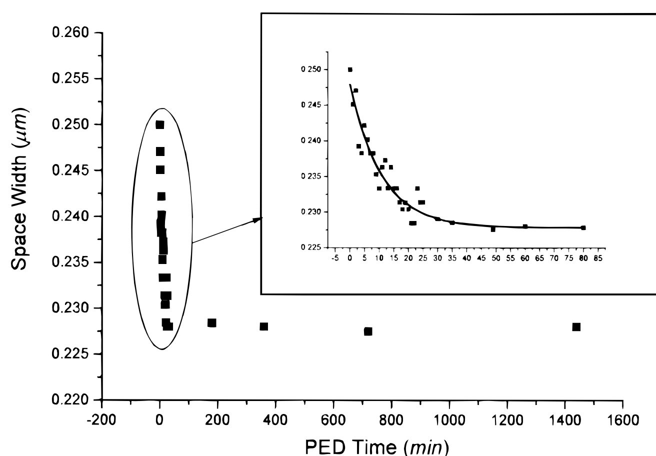

Figure 2. 0.25 μm space width for long-term PED.

resists included a t-BOC protected polystyrene base resin (substitution ratio around 25%) and an onium salt as a photoacid generator. Figure 1 schematically depicts the photolysis of the onium salt. The resist samples were coated on silicon substrates, which were hexamethyl disilazane (HMDS) vapor primed. The positive DUV resist was spin-coated to 0.6 μm thickness and prebaked at 110°C for 90 s. All patterns were exposed using a KrF excimer laser scanner with a 0.63 NA lens, and the PEB was carried out at 110°C for 90 s. The resist films were developed in 2.38 wt % tetramethylammonium hydroxide (TMAH) based developer for 60 s. A Hitachi S-8840 scanning electron microscope (SEM) was used to measure resist pattern linewidths. To prevent T-top formation, the concentration of ammonia was controlled below 8 ppb by mole in the air and below 0.8 ppb by mole within the track.

Sample analyses.—To investigate the influence of postexposure delay between exposure and postexposure bake (PEB), fourteen pattern sizes were exposed and patterns for different delay times that were measured separately. The measured lines or spaces, examined herein, were all line-and-space dense patterns. The relationships between linewidth and PED time for different linewidths have been established through the measurement of pattern widths.

Because the acid concentration corresponded with the aerial image of the resist, "space width" was measured and analyzed rather than linewidth in the following discussion. The aerial image simulation was carried out using a lithographic modeling tool PROLITH/2. Different levels of energy were exposed to assess how exposure energy affects the linewidth variation.

Results and Discussion

Behavior of space width according to PED time.—Figure 2 illustrates the measured 0.25 μm space width for different PED times. Obviously, the space width shrank immediately after exposure and eventually became saturated. Possibly, the circular dichroism (CD) change during PED was attributed to a T-top which is normally observed by increasing the time between the exposure and PEB process steps. To clarify the effect of airborne contamination, scanning electron micrograph (SEM) cross-sectional photographs of 0.18 and 0.25 μm line-and-space pattern profiles were verified under various PED times. Viewing the resist patterns presented in Fig. 3 and 4 confirmed that the line broadening during PED caused the space width shrinkage. The performance of T-top free resist patterns of organic-base added DUV resists were also consistent with the work of Kawai *et al*.[1] The above results indicated that the space width was not caused by the acid diffusion, because additional base component (NMP) not only quenched photogenerated acid, but also suppressed acid diffusion reaction within resist film.[8]

For a positive DUV resist, a radiation sensitive acid generator is decomposed during exposure, and the subsequent acid-catalyzed

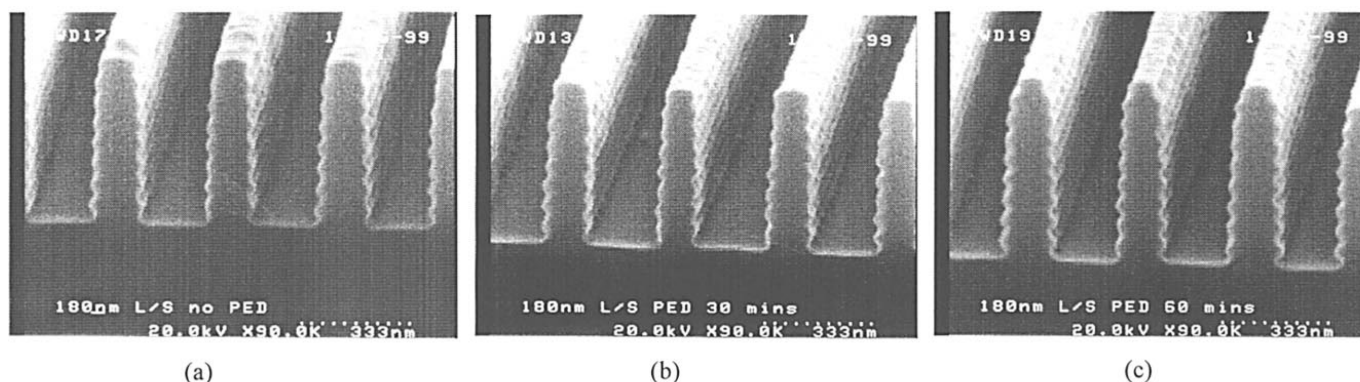

Figure 3. SEM photographs of 0.18 μm: (a) no PED delay, (b) PED of 30 min, and (c) PED of 60 min.

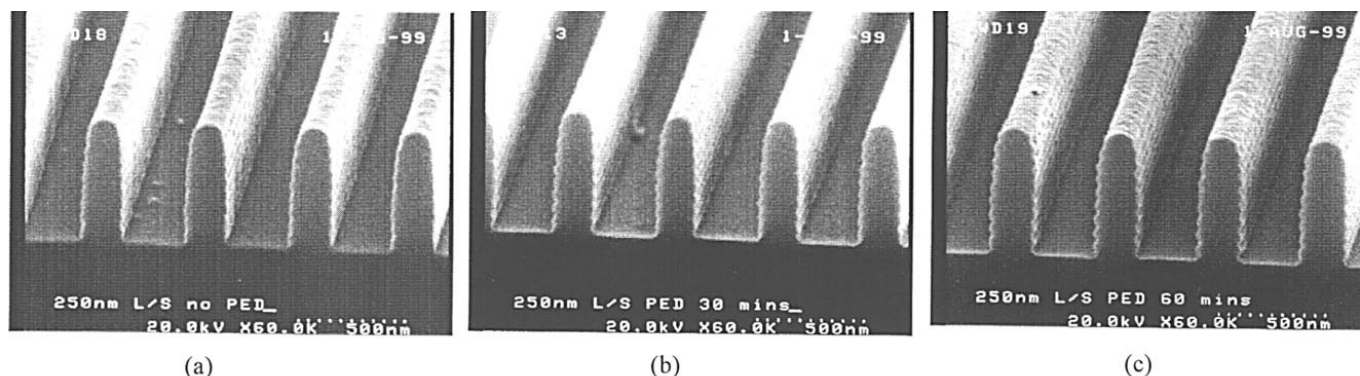

Figure 4. SEM photographs of 0.25 μm: (a) no PED delay, (b) PED of 30 min, and (c) PED of 60 min.

Downloaded on 2014-04-28 to IP 140.113.38.11 address. Redistribution subject to ECS terms of use (see ecsdl.org/site/terms_use) unless CC License in place (see abstract).

S0013-4651(99)09-090-4 CCC: $7.00 © The Electrochemical Society, Inc.

thermal reaction at elevated temperature makes the resist soluble. It is assumed herein that the added organic base neutralized some of the photogenerated acid and the depletion of acid reduced the space width. Figure 5 illustrates the schematic view of acid distribution in a chemically amplified resist with such an organic base. The photogenerated acid, created during DUV exposure, exists in two states, activated and deactivated. In Fig. 5, H^+ signifies the photogenerated acid, while "B" stands for the organic base which is originally added to the photoresist. In the activated state, the photogenerated acid decomposes polymers. However, the state becomes deactivated if the acid is trapped by the organic base.

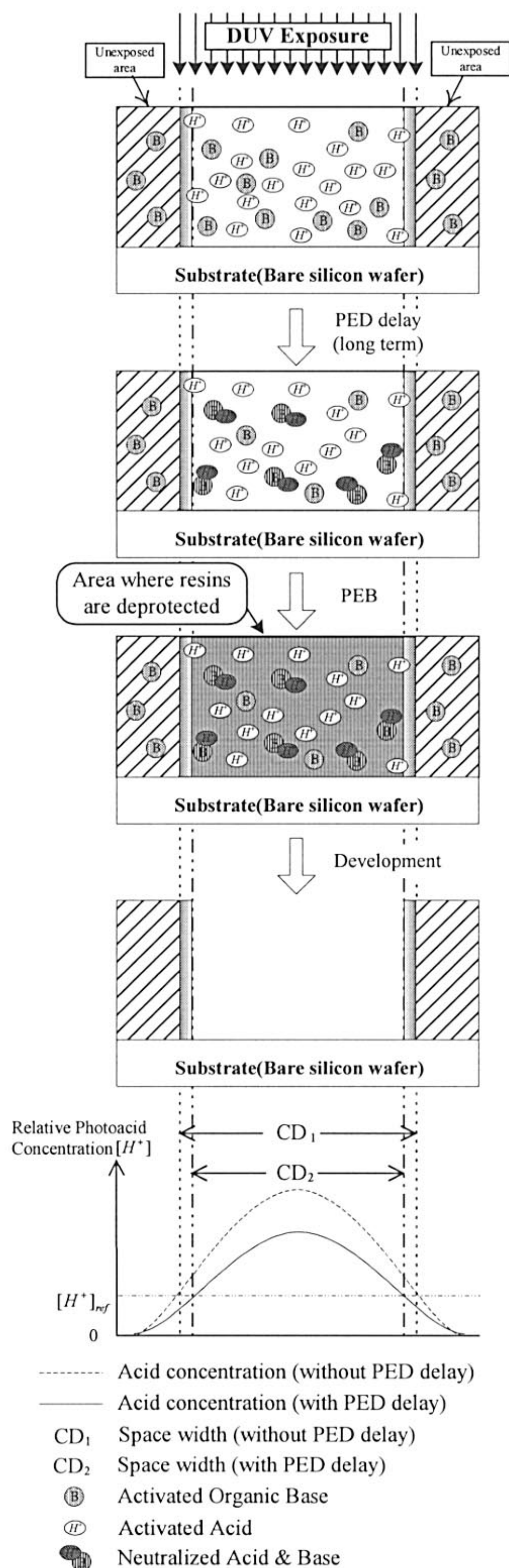

Figure 5. Distribution of photogenerated acid in the organic base added positive DUV resist.

During the postexposure bake (PEB), the catalytic reaction creates a large amount of deprotected resins within the exposed region (displayed in the middle potion of Fig. 5). Meanwhile, at the bottom of Fig. 5, the dashed line stands for initial acid concentration, while the solid line reflects the acid distribution after postexposure delay. The threshold acid concentration, $[H^+]_{ref}$, is the minimum acid concentration required to initiate cascading deprotection reactions during PEB to form a developable image. Because of the decrease in acid, the space width shrank from CD_1 to CD_2 when PED occurred. Although acid diffusion is necessary within the DUV-exposed region, to allow certain chemical reactions to occur, the behavior of the space width was dominated by the neutralization of acid and organic base rather than acid diffusion during post exposure delay.

To understand the behavior of space width during PED, the following section analyzes the influence of organic base. Herein, assume that the organic base concentration after delay t minutes is $[OH^-(t)]$, and the concentration of activated acid at time t is $[H^+(t)]$. Since the amount of active organic base at time t is related to itself, the base concentration $[OH^-(t)]$ can be described through the following relationship

$$\frac{d[OH^-(t)]}{dt} = -\frac{[OH^-(t)]}{\tau} \quad [1]$$

The concentration $[OH^-(t)]$ can be rewritten as

$$[OH^-(t)] = [OH^-(0)] \exp(-t/\tau) \quad [2]$$

The $[OH^-(0)]$ in Eq. 2 is the initial base concentration. Because some of the activated acid was neutralized by the organic base and became deactivated, the acid concentration at time t can be described by

$$[H^+(t)] = [H^+(0)] - \{[OH^-(0)] - [OH^-(t)]\} \quad [3]$$

Combining Eq. 2 and 3, the following relationship can be obtained

$$[H^+(t)] = [H^+(0)] + [OH^-(0)] \times \{\exp(-t/\tau) - 1\} \quad [4]$$

Because the acid distribution is defined by the aerial image of the resist, the space width $CD(t)$ and $CD(0)$ can be described by $[H^+(t)]$ and $[H^+(0)]$, respectively. The constant τ in Eq. 1 represents the time constant of organic base. To reveal the behavior of space width during PED, Eq. 4 can be transformed into the following equation

$$CD(t) = CD(0) + S[\exp(-t/\tau) - 1] \quad [5]$$

where the coefficient S is correlated to the initial active base concentration $[OH^-(0)]$.

Figure 6 summarizes the deviation of the space width, $CD(t)$-$CD(0)$, for 0.18, 0.2, and 0.3 μm pattern sizes. This figure demonstrates that the behavior of the space-width deviation according to PED time can be predicted effectively by the equation derived herein. The space width became saturated following approximately 30 to 40 min of postexposure delay. Therefore, the maximum space width the deviation for different pattern sizes was focused on herein, with this deviation occurring when the delay time t approaches infinity. The value of maximum deviation is the value of S in Eq. 5, and S can be described by the following relationship

$$S = CD(t = 0) - CD(t = \infty) \quad [6]$$

The lines in Fig. 6 denote the simulation results from Eq. 5 for different pattern sizes. Employing the curve-fitting technique allows the constant S to be obtained for various patterns. The average values of maximum space width variation, S_{ave}, were obtained from the measured CD of five levels of exposure energies, and the energy selection was based on the minimum mask bias for different pattern

Downloaded on 2014-04-28 to IP 140.113.38.11 address. Redistribution subject to ECS terms of use (see ecsdl.org/site/terms_use) unless CC License in place (see abstract).

S0013-4651(99)09-090-4 CCC: $7.00 © The Electrochemical Society, Inc.

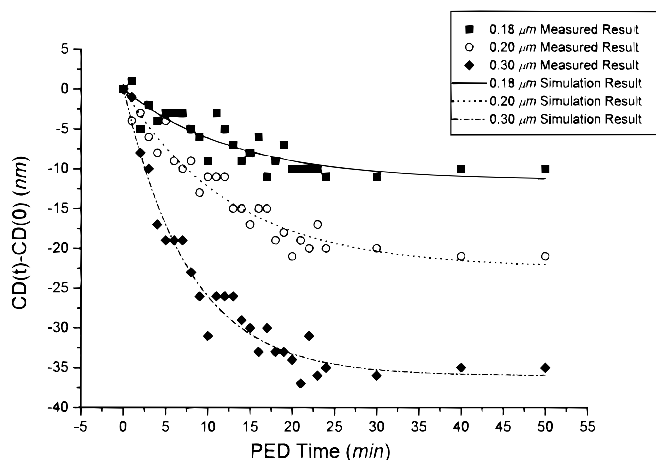

Figure 6. Deviation of space width, $CD(t)$-$CD(0)$, for 0.18, 0.2, 0.3 μm patterns.

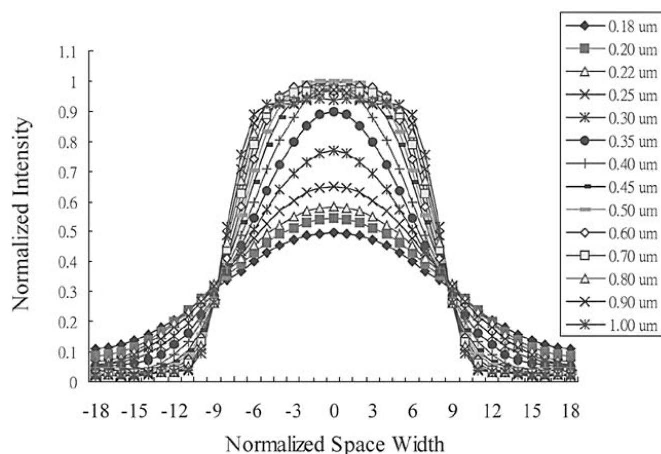

Figure 8. Intensity profile of normalized space width.

sizes. Figure 7 presents the maximum space-width S_{ave} for various pattern sizes. The highest value of S_{ave} ($S_{\text{ave,max}}$) is 30 nm, obtained at mask size of 0.45 μm.

The following section discusses the relationship between space-width variation and exposure energy.

Effect of energy on space width variation.—Figure 8 displays the normalized intensity profiles of the normalized space widths (I/I_{max}). The aerial image profiles were simulated using the modeling program PROLITH/2. The normalized peak intensity ($I_{\text{peak}}/I_{\text{peak,max}}$) decreases with the space width owing to light diffraction. To demonstrate the relationship between space-width variation and the effect of exposure energy, Fig. 9 illustrates the normalized maximum space-width variation ($S_{\text{ave}}/S_{\text{ave,max}}$) and normalized peak intensity ($I_{\text{peak}}/I_{\text{peak,max}}$).

The close relationship between these two curves means the peak intensity may correlate with the maximum space-width variation S, which represents the initial active base concentration $[OH^-(0)]$. Apparently, the value of S should be a constant value because the initial base concentration $[OH^-(0)]$ is the amount of the organic base, NMP, which was originally added to the resist. However, the experimental result will not conflict with the previous derivation if the mechanism of neutralization in the resist is analyzed. The work of Itani *et al.*,[8] confirmed that additional base components not only quenched photogenerated acid, but also suppressed acid diffusion reaction. During postexposure delay, some of the added base will "trap" the acid and become deactivated, while the organic base, which is left, will remain activated because of the limited acid diffusion length.[8] As Fig. 8 presents, the reduction of the latent acid image becomes more significant as the pattern size shrinks. Figures 10a and b illustrate the acid concentration for low and high exposure energies, respectively. The important point is that there is an equilibrium state between the activated and deactivated acids.[1] Thus, the neutralization process is reversible, *i.e.*, base (activated) + acid (activated) ⇄ neutralized (base + acid). During the postexposure delay, the organic base starts to trap the photogenerated acid when the acid is close to the base. Following a long-term PED, the concentration of activated and deactivated acids remain constant owing to the establishment of the equilibrium state. Figure 10 demonstrates that the activated base remaining in the low exposure energy condition exceeds that in the high exposure energy. Consequently, the "effective" base concentration is not a constant, and it decreases for lower acid concentration and lower exposure energy.

To further clarify the influence of exposure energy on space-width variation, the maximum space-width variations S were measured for different space widths. Figure 11 displays the energy dependence of space-width. Evidently, the maximum space-width variation S increased, as did the exposure energy, when the space width was below 0.5 μm. The intensity profiles shown in Fig. 8 clearly show that the acid concentration is much lower for a smaller space width, especially when the space width is close to the exposure wavelength (248 nm). Therefore, higher exposure energy could create more photogenerated acid, simultaneously increasing the effective base concentration. As Fig. 11 illustrates, raising the exposure energy can significantly increase the value of S for smaller space widths owing to the lower acid concentration. The effective base

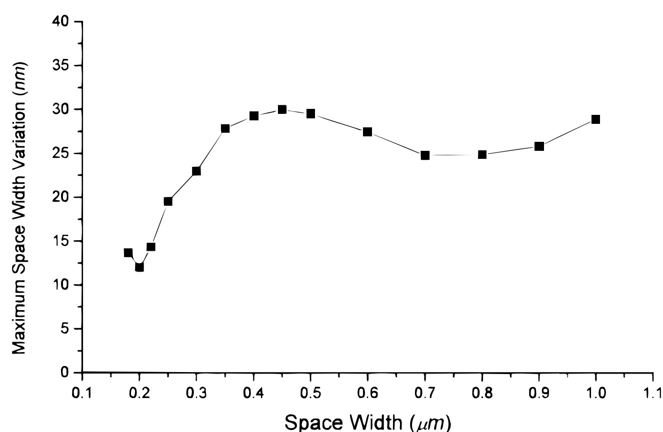

Figure 7. Maximum space width variation S_{ave} for different pattern sizes.

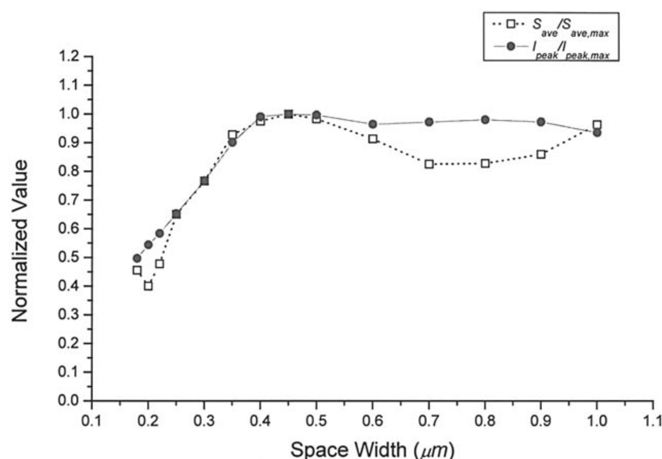

Figure 9. Relationship between normalized maximum space width variation ($S_{\text{ave}}/S_{\text{ave,max}}$) and normalized peak intensity ($I_{\text{peak}}/I_{\text{peak,max}}$).

Downloaded on 2014-04-28 to IP 140.113.38.11 address. Redistribution subject to ECS terms of use (see ecsdl.org/site/terms_use) unless CC License in place (see abstract).

S0013-4651(99)09-090-4 CCC: $7.00 © The Electrochemical Society, Inc.

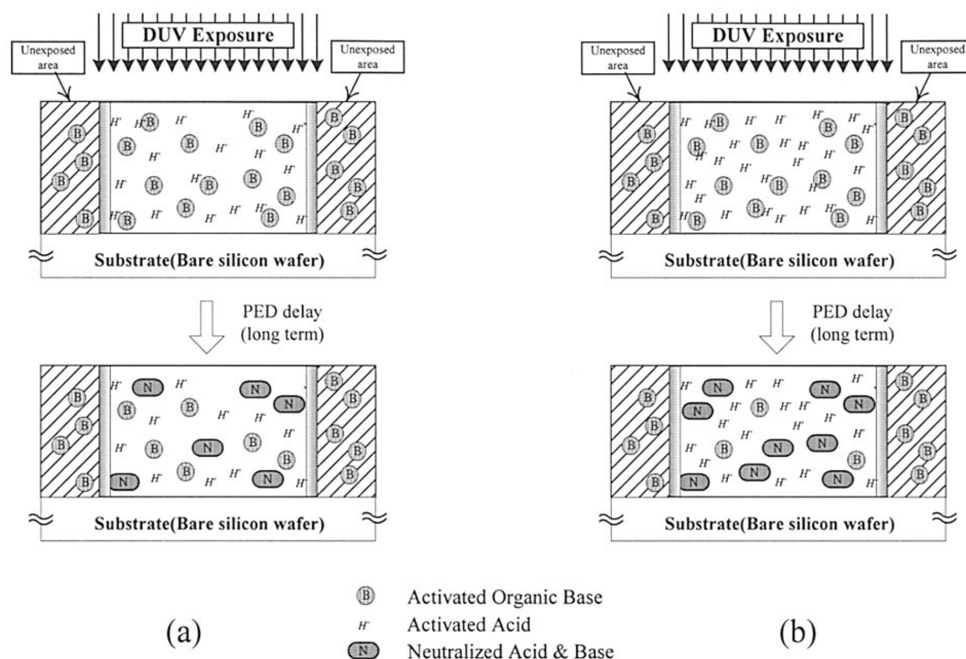

Figure 10. Acid concentration for (a) low exposure energy and (b) high exposure energy.

concentration is higher for the larger space width owing to resist film containing more acid. Therefore, the energy dependency for the larger space is less evident than for the smaller space width.

The above discussion demonstrates that $[OH^-(t)]$ should be treated as an effective base concentration, and the model proposed herein can effectively characterize the behavior of space-width variation.

Evaluation of the time constant "τ".—Comparing the experimental data and simulation results shown in Fig. 6 revealed that the space-width variation, $CD(t)$-$CD(0)$, could be precisely described by Eq. 5 according to PED time. From the previous derivation, τ was known to be the time constant of the organic base, representing how fast the photogenerated acid reacted with the organic base. Thus, the active base concentration would be $[OH^-(0)]e^{-1}$, if the PED time equaled the time constant τ. Employing the concept of effective base concentration, the time constant τ was assumed to be a constant value for different space widths and exposure energies. The values of time constant τ were obtained by averaging the τ for different levels of exposure energy. Figure 12 displays the values of τ, with the average being around 10 min. To verify the influence of time constant τ, Fig. 13 displays the simulation results. Clearly, the simulation curves can still match the experimental results despite the time constant ranging from 7 to 12 min. Possibly the fluctuation of the time constant τ was caused by measurement error. Alternatively, the model presented herein can be further improved to more precisely describe the space-width variation. However, introducing the concept of effective base concentration remains appropriate due to the close correlation between experimental and simulated results.

Application of PED on EL and DOF.—The result of the section of Effect of energy on space-width variation demonstrates that the higher the exposure energy, the larger the value of S. By applying the property of energy dependence to the space-width variation, the EL and DOF can be extended.

Assume that 0.18 μm line-and-space patterns are exposed by two energy levels, E_1 and E_2 ($E_1 > E_2$). The measured space widths are CD_1 and CD_2 for energy E_1 and E_2, respectively. CD_1 is larger than CD_2 owing to the higher exposure energy. The difference between the two space widths is

$$\Delta CD = CD_1 - CD_2 > 0 \quad [7]$$

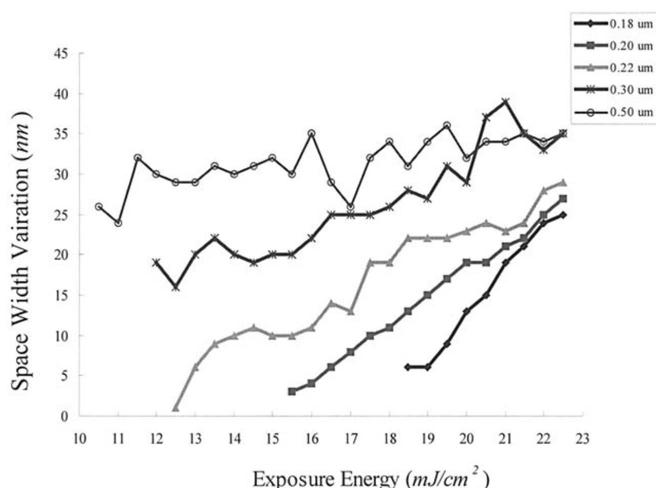

Figure 11. Maximum space width variation, S, for different space widths at energy levels ranging form 10.5 to 22.5 mJ/cm^2.

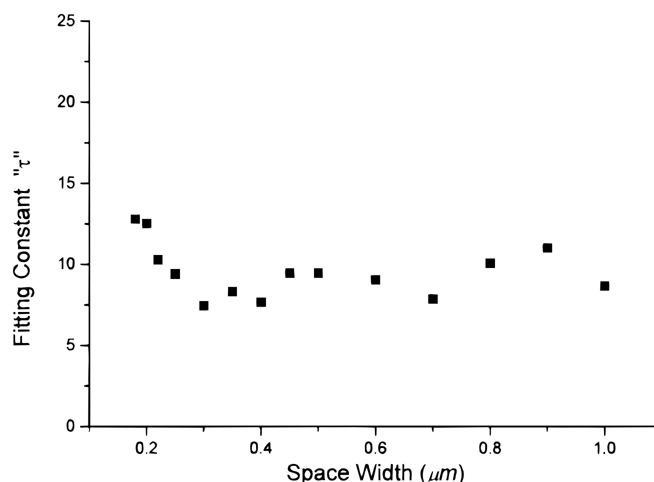

Figure 12. Fitting constant τ for different space widths.

Downloaded on 2014-04-28 to IP 140.113.38.11 address. Redistribution subject to ECS terms of use (see ecsdl.org/site/terms_use) unless CC License in place (see abstract).

S0013-4651(99)09-090-4 CCC: $7.00 © The Electrochemical Society, Inc.

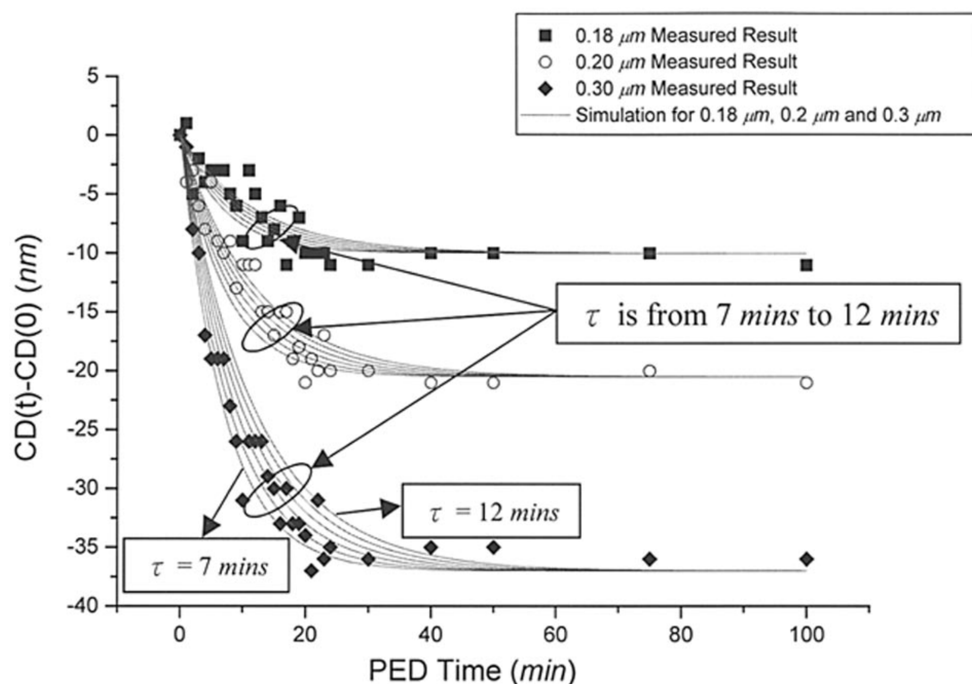

Figure 13. Simulation results of different levels of time constant τ for 0.18, 0.2, and 0.3 μm patterns. (τ ranges from 7 to 12 min.)

If both patterns have a long-term postexposure delay, the space widths will be saturated and become a constant. Assume the space width variations are S_1 for CD_1 and S_2 for CD_2. The value of S_1 is larger than the value of S_2, because the value of S is larger for the higher exposure energy. Therefore, the space-width difference, which has a PED, between the two energy levels, is

$$\Delta CD' = (CD_1 - S_1) - (CD_2 - S_2) = \Delta CD - (S_1 - S_2) < \Delta CD \quad [8]$$

Because the value of $\Delta CD'$ is smaller than ΔCD, it was concluded that space width is insensitive to exposure energy, and the exposure latitude could be extended when the exposed patterns have the PED.

To ensure that the postexposure delay will benefit the process, 0.18 μm line-and-space patterns are exposed for different levels of energy. Figure 14 displays the difference between the measured CD and mask CD for different exposure energies. Evidently the slope is steeper for the patterns that have no postexposure delay. This phenomenon implies the change of space width is less sensitive to the change in exposure energy under a PED condition. Figure 15 shows the exposure latitude of the 0.18 and 0.22 μm patterns for different DOF based on the ±10% of the nominal CD. Normally, the 10% exposure latitude is the minimum requirement for mass production. Table I is the measured DOF for 0.18 and 0.22 μm patterns based on the 10% EL criterion. Using the PED, the DOF improvement of the 0.18 and 0.22 μm patterns are 50 and 37.5%, respectively.

From the previous results, it was concluded that exposure latitude and DOF can be extended via postexposure delay for organic-base added DUV resists.

Conclusions

This work investigated how base additive affects linewidth variation and lithographic performance in t-BOC protected-type chemically amplified positive DUV resist. Clear relationships among space width variation, PED duration, and the effect of additional organic base on space width were identified. An exponential equation was also derived to accurately describe the behavior of space width according to PED time. Based on the analysis of experimental results and intensity profile simulation, we conclude that maximum space-width variation is controlled by acid concentration in resist film. Finally, the PED effect can be employed to extend the exposure latitude and depth of focus.

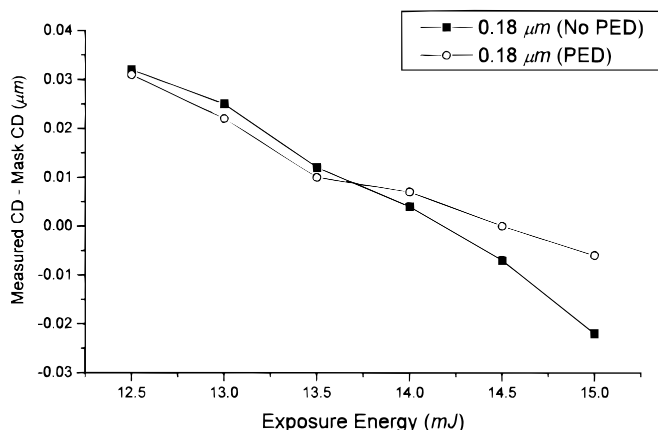

Figure 14. Difference between measured CD and mask CD for 0.18 μm patterns.

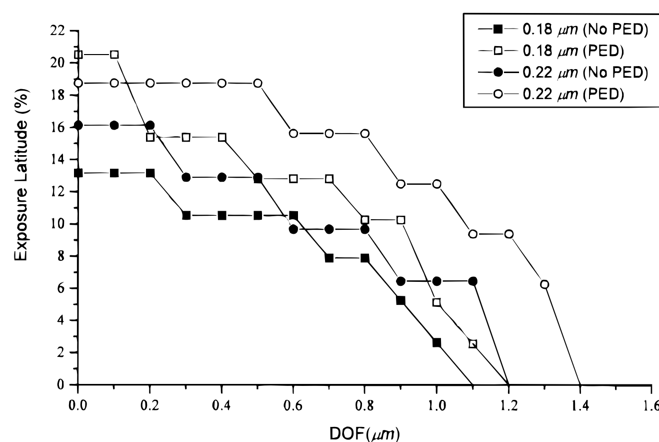

Figure 15. EL of 0.18 and 0.22 μm patterns.

Downloaded on 2014-04-28 to IP 140.113.38.11 address. Redistribution subject to ECS terms of use (see ecsdl.org/site/terms_use) unless CC License in place (see abstract).

S0013-4651(99)09-090-4 CCC: $7.00 © The Electrochemical Society, Inc.

Table I. DOF of 0.18 and 0.22 μm line-and-space patterns with 10% exposure latitude (EL).

	Without PED delay (μm)		With PED delay (μm)	
Linewidth	0.18	0.22	0.18	0.22
DOF	~0.6	~0.8	~0.9	~1.1

Acknowledgments

The authors would like to thank the National Science Council of Taiwan for financially supporting this research under contract no. 88-2215-E009-045.

National Chiao Tung University assisted in meeting the publication costs of this article.

Reference

1. Y. Kawai, A. Otaka, A. Tanaka, and T. Matsuda, *Jpn. J. Appl. Phys.*, **33**, 7023 (1994).
2. S. A. MacDonald, N. J. Clecak, H. R. Wendt, C. G. Willson, C. D. Snyder, C. J. Knors, N. B. Deyoe, J. G. Maltabes, J. R. Morrow, A. E. McGuire, and S. J. Holmes, *Proc. SPIE-Int. Soc. Opt. Eng.*, **1466**, 2 (1991).
3. T. Kumada, Y. Tanaka, A. Ueyama, S. Kubota, and H. Koezuka, *Proc. SPIE-Int. Soc. Opt. Eng.*, **1925**, 31 (1993).
4. A. Oikawa, N. Santoh, and S. Miyata, *Proc. SPIE-Int. Soc. Opt. Eng.,* **1925**, 92 (1993).
5. T. Fischer, U. Boettiger, A. Grassmann, H. Moritz, H. Binder, D. Funhoff, and R. Schwalm, *Microelectron. Eng.*, **23**, 311 (1994).
6. V. Deshpande, N. Thane, J. Hargreaves, Y. Takamori, and E. Apelgren, *Proc. SPIE-Int. Soc. Opt. Eng.,* **1926**, 208 (1993).
7. K. J. Przybilla, Y. Kinoshita, T. Kudo, S. Masuda, H. Okazaki, M. Padmanaban, G. Pawlowski, J. Roeschert, W. Spiess, and N. Suehiro, *Proc. SPIE-Int. Soc. Opt. Eng.,* **1925**, 76 (1993).
8. T. Itani, H. Yoshino, S. Hashimoto, M. Yamana, N. Samoto, and K. Kasama, *Microelectron. Eng.*, **35**, 149 (1997).
9. T. Itani, H. Iwasaki, M. Fujimoto, and K. Kasama, *Jpn. J. Appl. Phys.*, **33**, 7005 (1994).
10. T. Itani, H. Yoshino, S. Hashimoto, M. Yamana, N. Samoto, and K. Kasama, *Jpn. J. Appl. Phys.*, **35**, 6501 (1996).
11. T. H. Fedynyshyn, J. W. Thackeray, J. H. Georger, and M. D. Denison, *J. Vac. Sci Technol. B*, **12**, 3888 (1994).
12. T. Itani, H. Yoshino, M. Fujimoto, and K. Kasama, *J. Vac. Sci. Technol. B*, **13**, 3026 (1995).
13. T. Yoshimura, H. Shiraishi, and S. Okazaki, *Jpn. J. Appl. Phys.*, **34**, 6786 (1995).
14. G. M. Wallraff, W. D. Hinsberg, F. A. Houle, M. Morrison, C. E. Larson, M. Sanchez, J. Hoffnagle, P. J. Brock, and G. Breyta, *Proc. SPIE-Int. Soc. Opt. Eng.,* **3678**, 138 (1999).
15. J. Kim, Y. Kwon, J. Choi, and M. Jung, *Proc. SPIE-Int. Soc. Opt. Eng.,* **3678**, 536 (1999).
16. J. L. P. Jessop, S. N. Goldie, A. B. Scranton, G. J. Blanchard, B. Rangarajan, L. Capodieci, R. Subramanian, and M. K. Templeton, *Proc. SPIE-Int. Soc. Opt. Eng.,* **3678**, 914 (1999).
17. X. Shi, *Proc. SPIE-Int. Soc. Opt. Eng.,* **3678**, 342 (1999).
18. J. Nakamura, H. Ban, K. Deguchi, and A. Tanaka, *Jpn. J. Appl. Phys.*, **30**, 2619 (1991).
19. J. S. Petersen, C. A. Mark, J. Sturtevant, J. D. Byers, and D. A. Miller, *Proc. SPIE-Int. Soc. Opt. Eng.,* **2438**, 167 (1995).
20. J. Nakamura, H. Ban, and A. Tanaka, *Jpn. J. Appl. Phys.*, **33**, 6368 (1994).
21. L. Ferreira, S. Malik, T. R. Sarubb, A. J. Blakeney, and B. Maxwell, *Proc. SPIE-Int. Soc. Opt. Eng.,* **3333**, 236 (1998).
22. T. H. Fedynyshyn, C. R. Szmanda, R. F. Blacksmith, W. E. Houck, and J. C. Root, *J. Vac. Sci. Technol. B*, **11**, 2798 (1993).
23. G. Arthur, N. Eilbeck, and B. Martin, *Microelectron. Eng.*, **35**, 137 (1997).
24. D. J. H. Funhoff, H. Binder, and R. Schwalm, *Proc. SPIE-Int. Soc. Opt. Eng.,* **1672**, 46 (1992).
25. W. S. Huang, *Proc. SPIE-Int. Soc. Opt. Eng.,* **3678**, 1040 (1999).
26. J. Nakamura, H. Ban, and A. Tanaka, *Jpn. J. Appl. Phys.*, **31**, 4294 (1992).
27. T. Itani, H. Yoshino, S. Hashimoto, M. Yamana, N. Samoto, and K. Kasama, *Photopolym. Sci. Technol.*, **10**, 409 (1997).

Downloaded on 2014-04-28 to IP 140.113.38.11 address. Redistribution subject to ECS terms of use (see ecsdl.org/site/terms_use) unless CC License in place (see abstract).